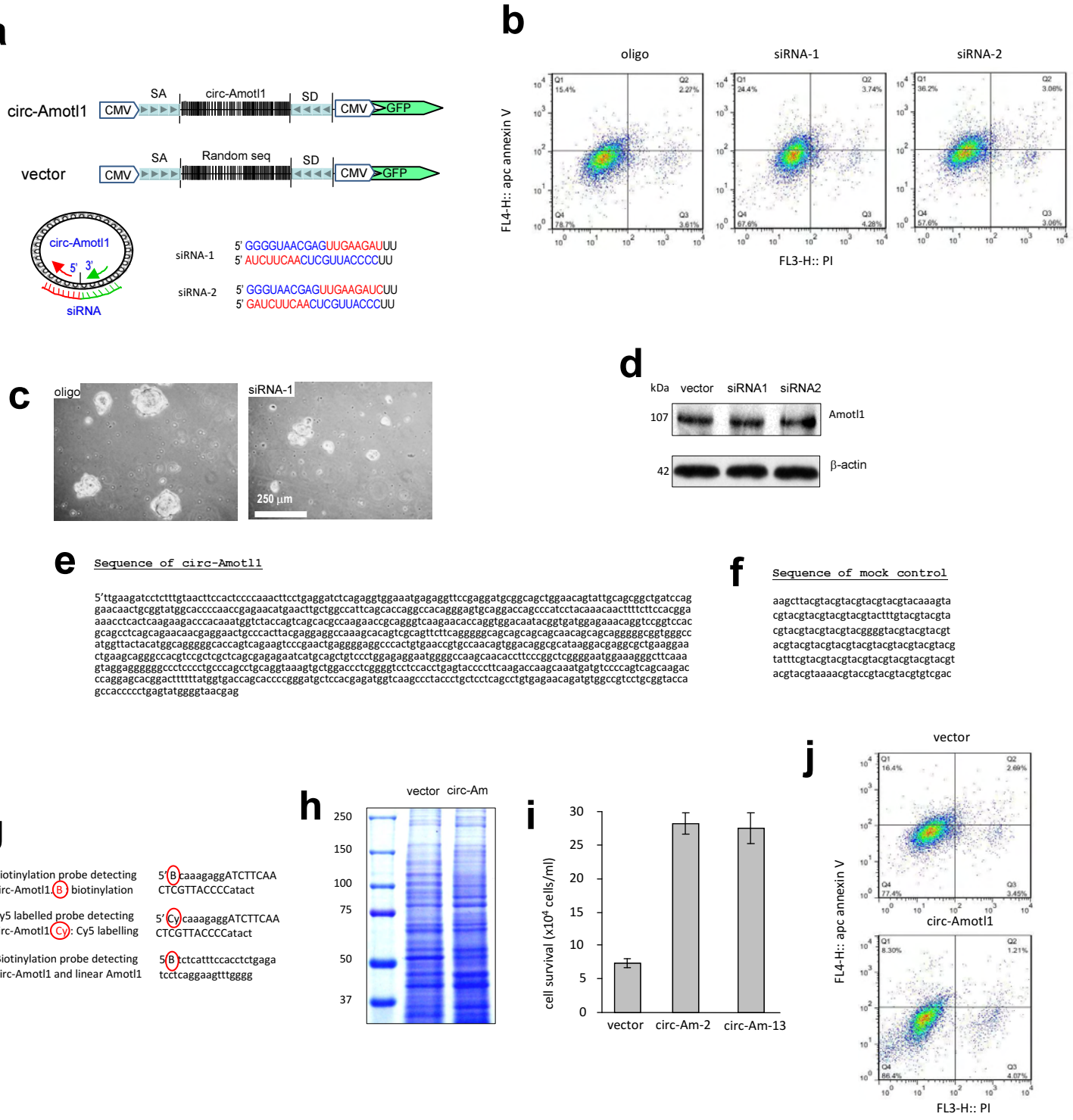

Supplementary Fig S1. Cell activities affected by circ-Amotl1 expression.
(a) Diagram of circ-Amotl1 expression construct and siRNA sequences specific to circ-Amotl1.
(b) The control oligo or circ-Amotl1 siRNA-transfected MDA-MB-231 cells were cultured in serum-free DMEM for 3 days, and subject to Annexin V staining, followed by flow cytometry. Typical pictures showed that anti-circ-Amotl1 siRNA-transfected MDA-MB-231 cells had more Annexin V staining.
(c) Human breast cancer cells (MCF-7) were inoculated in 12-well plate (5 x10⁴ cells/ml/well) and incubated overnight. The cultures were transfected with the siRNA and the control oligo. After transfection, the cultures were maintained in agarose gel for colony formation. Transfection with siRNA targeting circ-Amotl1 decreased colony forming capacity.
(d) Western blot showing that protein levels of Amotl1 was not affected by siRNA transfection.
(e) Sequences of circ-Amotl1 expression construct.
(f) Sequences of mock control.
(g) Sequences of probes specifically targeting circ-Amotl1 and a probe recognizing circ-Amotl1 and linear Amotl1 mRNA.
(h) SDS-PAGE of total proteins from circ-Amotl1- and vector-transfected cells.
(i) The vector- and circ-Amotl1-transfected MDA-MB-231 cells were maintained in tissue culture dishes in serum-free conditions for cell survival assay. Transfection with circ-Amotl1 enhanced cell survival.
(j) The circ-Amotl1- and vector-transfected MDA-MB-231 cells were cultured in serum-free DMEM for 3 days, and subject to Annexin V staining, followed by flow cytometry. Typical pictures showed that the circ-Amotl1-transfected MDA-MB-231 cells had less Annexin V staining.

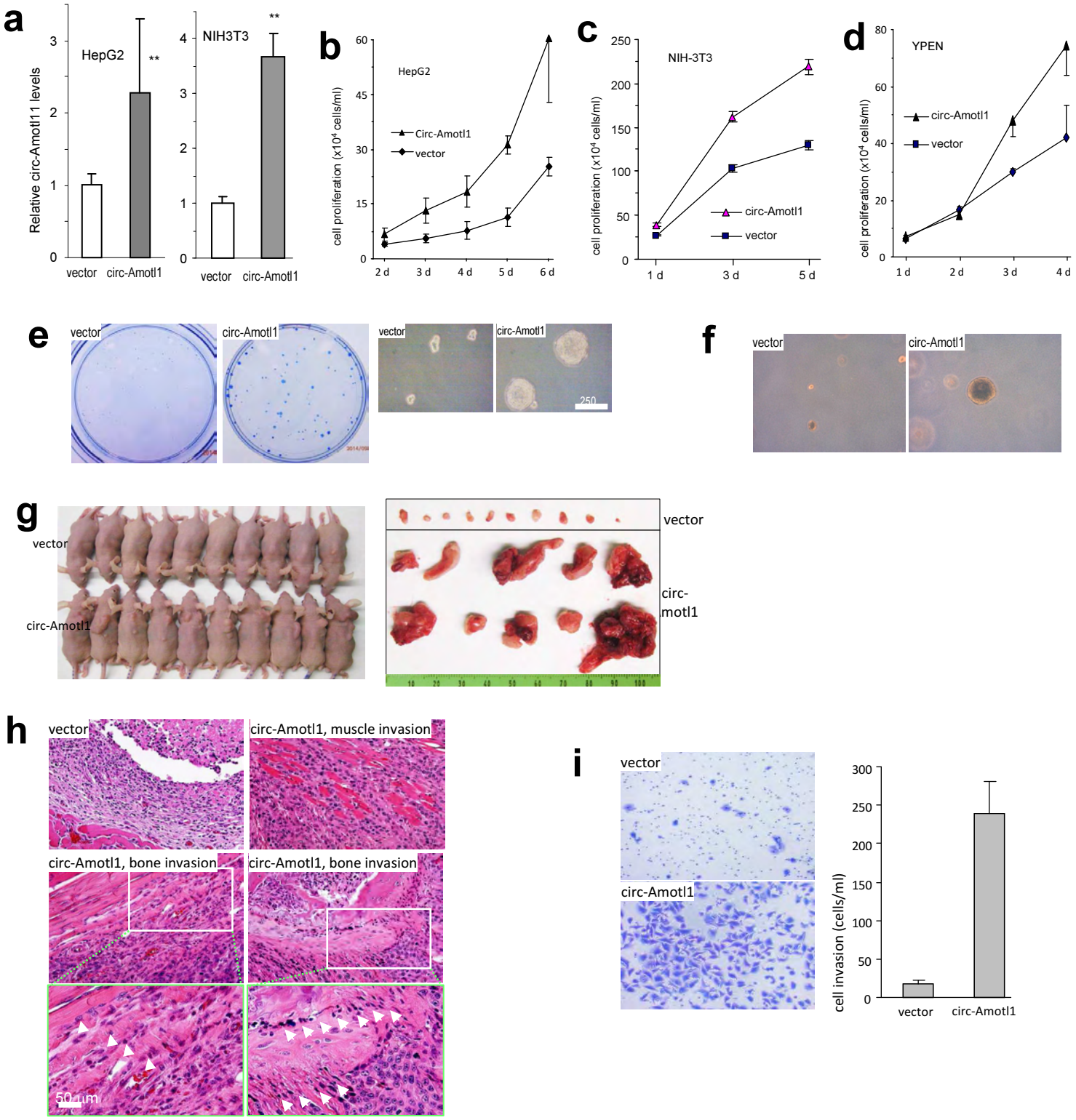

Fig S2. Tumor growth and cell invasion affected by circ-Amotl1 expression

(a) Expression of circ-Amotl1 in HepG2 and NIH3T3 analyzed by real-time PCR.

(b-d) Cell proliferation was assayed in vector- and circ-Amotl1-transfected HepG2 cells (b), NIH3T3 fibroblasts (c), and YPEN cells (d). Cells transfected with circ-Amotl1 displayed increased proliferation.

(e) The cells transfected with circ-Amotl1 formed much larger colonies than the vector-transfected cells.

(f) The circ-Amotl1-transfected HepG2 cells formed larger colonies than the control when the cells were plated agarose with 10% FBS

(g) Left, MDA-MB-231 cells transfected with circ-Amotl1 or the vector were injected subcutaneously into nude mice. Tumor growth was monitored for 17 days. Expression of circ-Amotl1 increased tumor growth. Right, Tumors were isolated from the mice.

(h) The H&E stained tumor sections were examined under a light microscope. Extensive cell death was detected in the control tumors but not in the circ-Amotl1 tumors. In the circ-Aomotl1 tumors, the cells invaded into muscle and bone tissues.

(i) The vector- and circ-Amotl1-transfected MDA-MB-231 cells ($1x10^5$ cells) were incubated in Matrigel for 24 h for cell invasion assays. Expression of circ-Amotl1 enhanced cell invasion.

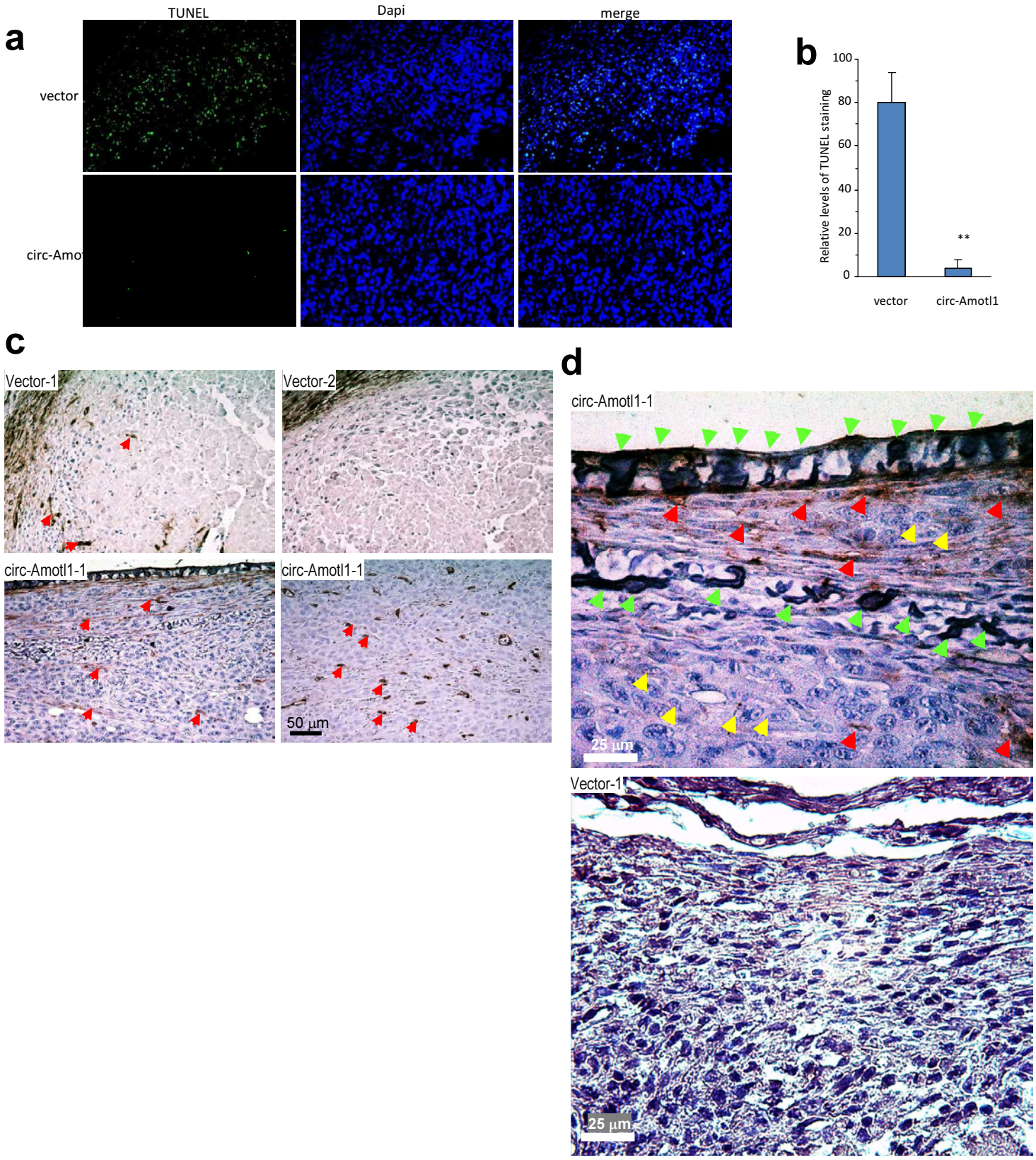

Fig S3. Tumor section staining

(a) Tumor sections were subject to TUNEL staining to analyze cellular apoptosis. There were few apoptotic cells in the tumors formed by the circ-Amotl1-transfected cells. However, extensive apoptotic cells were detected in the tumor sections of the control group.

(b) Quantitation analysis showed more than 20-fold decrease in apoptosis of the circ-Amotl1 tumor sections compared with the control ($p=0.00014$, $n=4$ scans).

(c) Tumor sections were subject to immunohistochemical staining for CD34 expression. Extensive CD34 positive cells were detected in the circ-Amotl1 tumors but not in the control.

(d) Tumor sections from circ-Amotl1 or control tumors, after CD34 staining, showed that the bone (green arrows) was broken down by tumor cells (yellow arrows). The CD34 positive cells (red arrows) migrated into the bone tissue, which were not detected in the tumors formed by the vector-transfected cells.

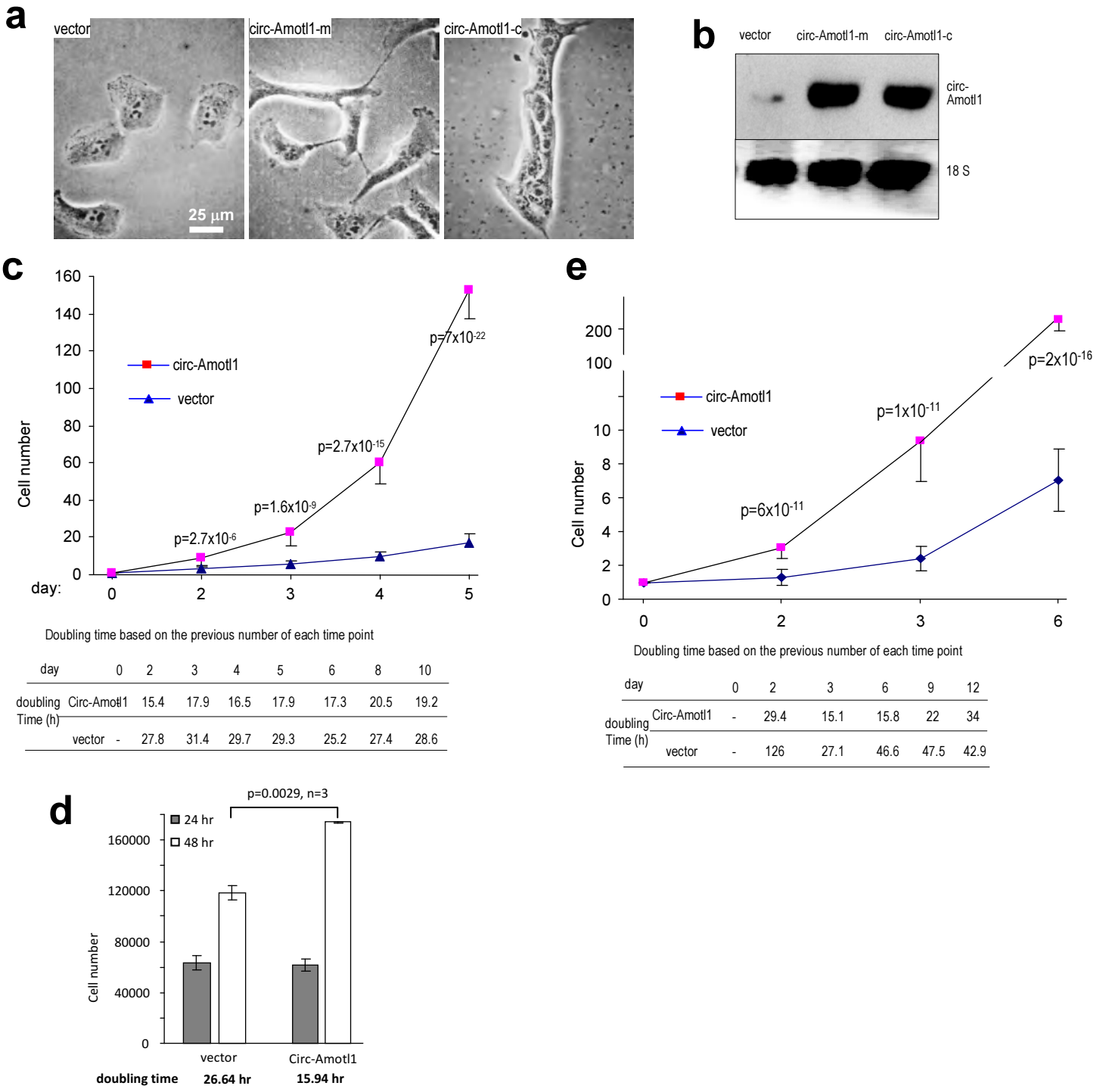

Fig S4. Purification of circ-Amotl1 cell lines

(a) Morphology of cells from vector-transfection, a cell line isolated from circ-Amotl1 transfection (mix population, circ-Amtol1-m), and a colony from circ-Amotl1-transfected cells (circ-Amotl1-c).

(b) Total RNA extracted was subject to Northern blot with a probe specific to circ-Amotl1, showing increased expression of circ-Amotl1.

(c) Upper, Single cell growth curve in the early stages. Significant difference (p=0.0000027) was obtained on day 2 (n=20 wells). Lower, doubling time for single cell growth curve, using previous cell number for the calculation.

(d) Population doubling time. $5x10^4$ cells were inoculated in 6-well plates. Cell number was determined at 24 h and 48 h, respectively. The difference in cell number between 24 and 48 h was used to calculated population doubling time.

(e) Upper, Colony growth curve in the early stages. Significant difference ($p=6x10^{-11}$) was obtained on day 2 (n=20 colonies). Lower, doubling time for colony growth curve, using previous cell number for the calculation.

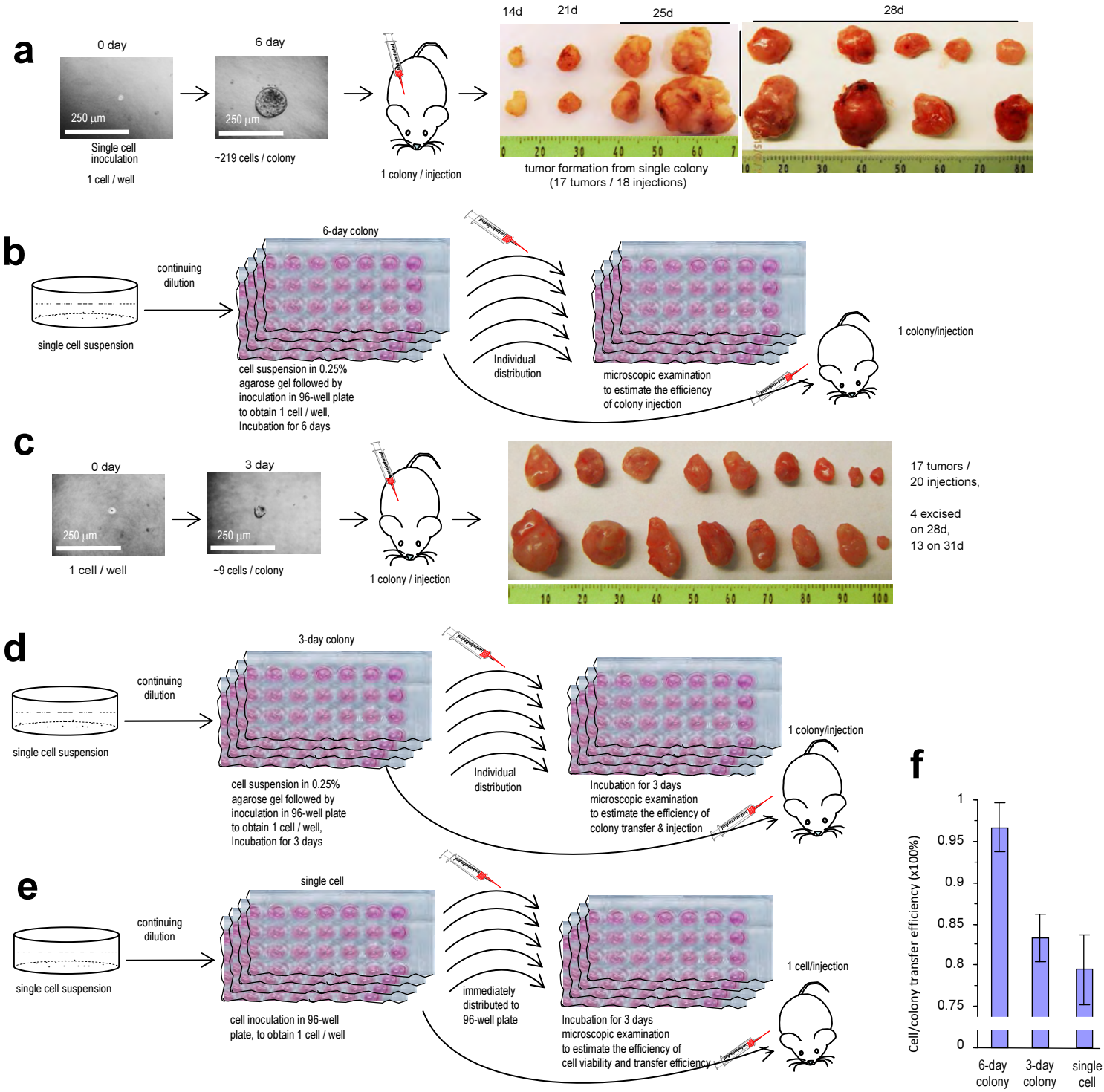

Fig S5. Efficiencies of cell growth, transfer, and tumor formation

(a) Six days after single cell inoculation, colonies (~219 cells/colony) were injected into mice (1 colony/well/injection). In the control, 500, 5,000, and 50,000 vector-transfected cells were injected (n=5). Tumors were isolated on the days as indicated.

(b) Transfer efficiency. Six days after single cell inoculation, colonies formed in 96-well plates were transferred, one-by-one in the same manner as mouse injection. After transfer, the number of colonies in the new plates was examined under a light microscope to estimate the efficiency of colony transfer. While the efficiency of transfer was 100%, we estimated a 5% technical accident could occur during the process.

(c) Three days after inoculation, colonies (~9 cells/colony) were injected into mice (1 colony/well/injection). In the control, 500, 5,000, and 50,000 vector-transfected cells were injected. Tumors were isolated on days 28 and 31.

(d) Three days after single cell inoculation, colonies formed in 96-well plates were transferred. After transfer, the colonies in the new plates were allowed to grow for an additional 3 days, so that the size of each colony could be seen easier under a light microscope. We could obtain an efficiency of approximately 85% for the transfer/injection.

(e) Viability and transfer efficiency of single cell. Single cell suspension was distributed into 96-well plates. The wells that contained a single cell were marked. Medium and the cell were transferred to a well in a new plate. After transfer, the cell was allowed to grow for 3-4 days. We could only obtain an efficiency of 80% for the transfer/injection.

(f) Summary of transfer efficiencies for colony and single cells.

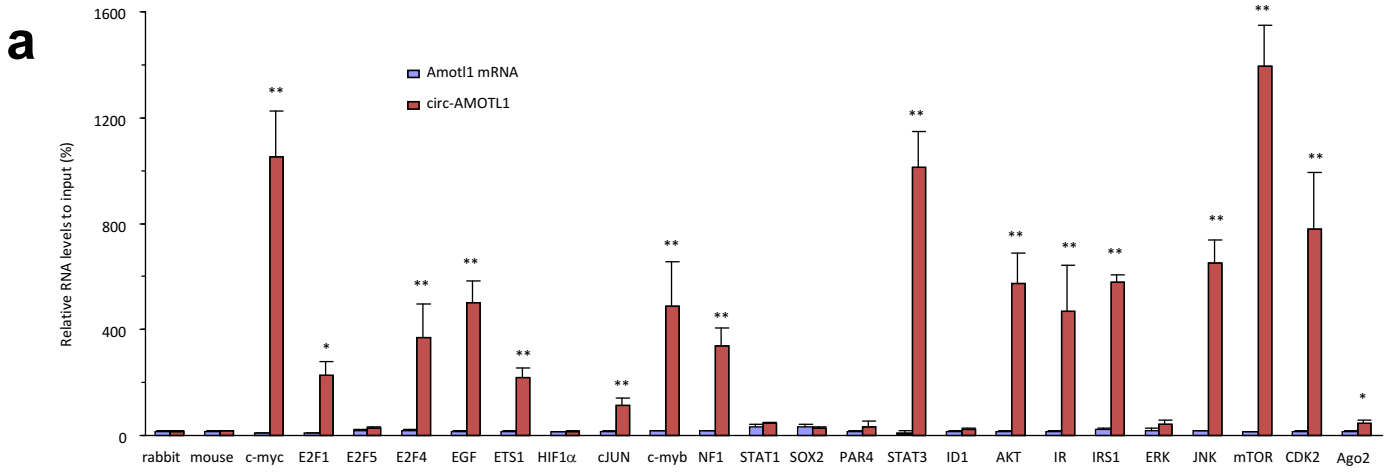

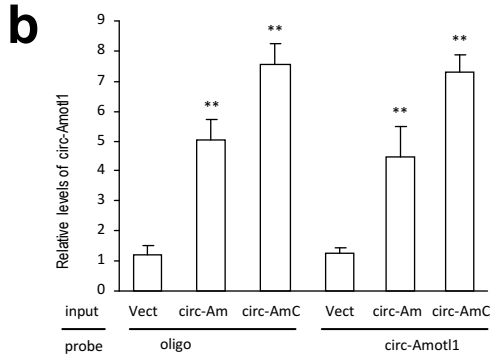

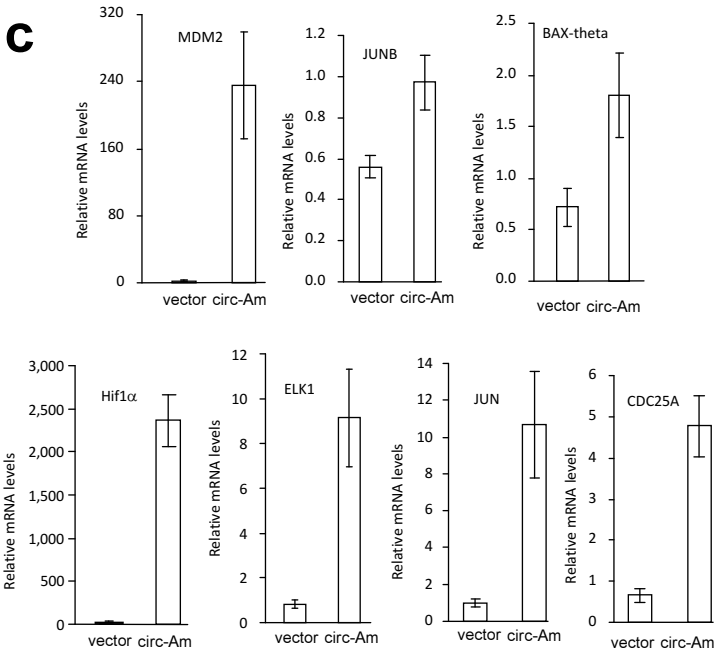

d

Primers used in this study

primer	sequence	product
hu.HIF1a-promot-F	5′ cgtcccagctgtgcctcagctgac	HIF1α promoter
hu.HIF1a-promot-R	5′ gcaagggcggaggcgcgctcgggc	
hu.Cdc25a-promot-F	5′ ccaataagggctagaatggaagtg	Cdc25a promoter
hu.Cdc25a-promot-R	5′ ctaaccgtgcagtattgtggaccc	
hu.Mdm2-promot-F	5′ gtgagccaccgcgcccagccaaac	Mdm2 promoter
hu.Mdm2-promot-R	5′ ctccaccagccgctggagttgtac	
hu.Elk1-promot-F	5′ cgacccactcccgccggctgctac	Elk1 promoter
hu.Elk1-promot-R	5′ gcctcacactgattggcttacatg	
hu.JUN-promot-F	5′ cctccatcagaggttgcgagcgtc	JUN promoter
hu.JUN-promot-R	5′ gaggctcacgggatgaggtaatgc	
hu.JUNB-promot-F	5′ cttcctgacagtgacgcgagccgc	JUNB promoter
hu.JUNB-promot-R	5′ cagctcccagctccctgctggctc	
hu.cir.Amotl1-R	5′ cctggatcagccgctgcaatactgttccagc	Amotl1 pre-mRNA
hu.Amotl1-intron-F	5′ gacatatatctcctgtggagctgc	
cir-Amo-FMut	5′ gcccacgcgtacagtattaaagcggctgatccaggaa	mutated circ-Amotl1
cir-Amo-RMut	5′ gcccacgcgttgaatcatcctcttaacctctcatttcc	

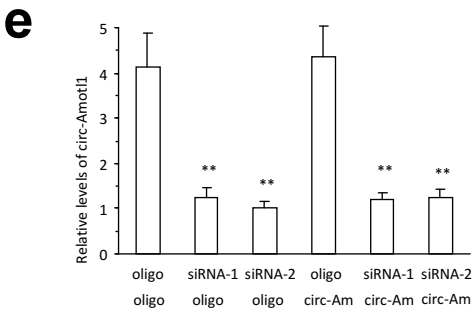

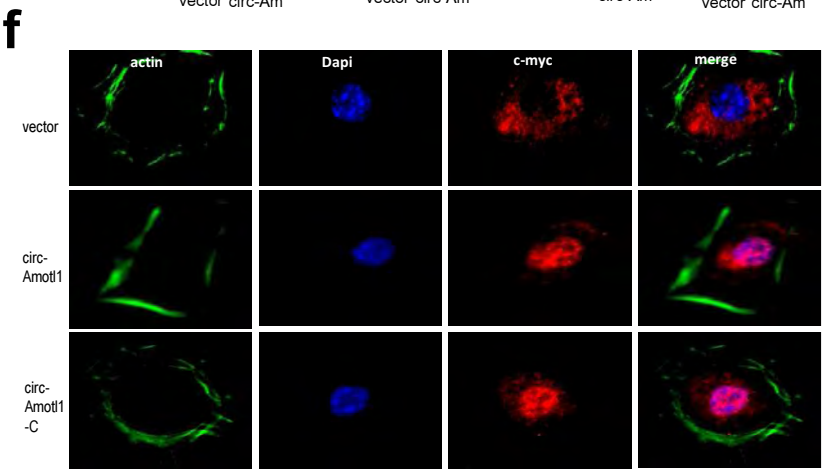

Fig S6. siRNA targeting circ-Amotl1

(a) MDA-MB-231 cell lysate was incubated with antibodies as indicated to analyze the interaction of circ-Amotl1 with more oncogenic proteins. **, *p<0.01*. Error bars, SD (*n=4*).

(b) Lysates of vector- and circ-Amotl1-transfected cells were mixed with a biotinylated DNA oligo probe complementary to circ-Amotl1 or a control oligo and the mixtures were subject to real-time PCR to confirm equal amounts of circ-Amotl1 input in the reactions.

(c) The circ-Amotl1- and vector-transfected MDA-MB-231 cells were grown to 100% confluence followed by RNA extraction. The circ-Amotl1-transfected cells expressed significantly higher levels of c-myc targets than the control.

(d) Sequences of primers used to amply the promoters.

(e) Cells were transfected with siRNAs targeting circ-Amotl1 or a control oligo. Cell lysate was prepared and mixed with the probe and the mixtures were subject to real-time PCR to confirm equal amounts of circ-Amotl1 input in the reactions.

(f) The mock- and circ-Amotl1-transfected MDA-MB-231 cells were immuno-stained with phalloidins (green), DAPI (blue), and c-myc (red). High intensity of c-myc was detected in the nucleus of the circ-Amotl1-transfected cells, but most of c-myc was detected in the cytoplasm of the control cell.

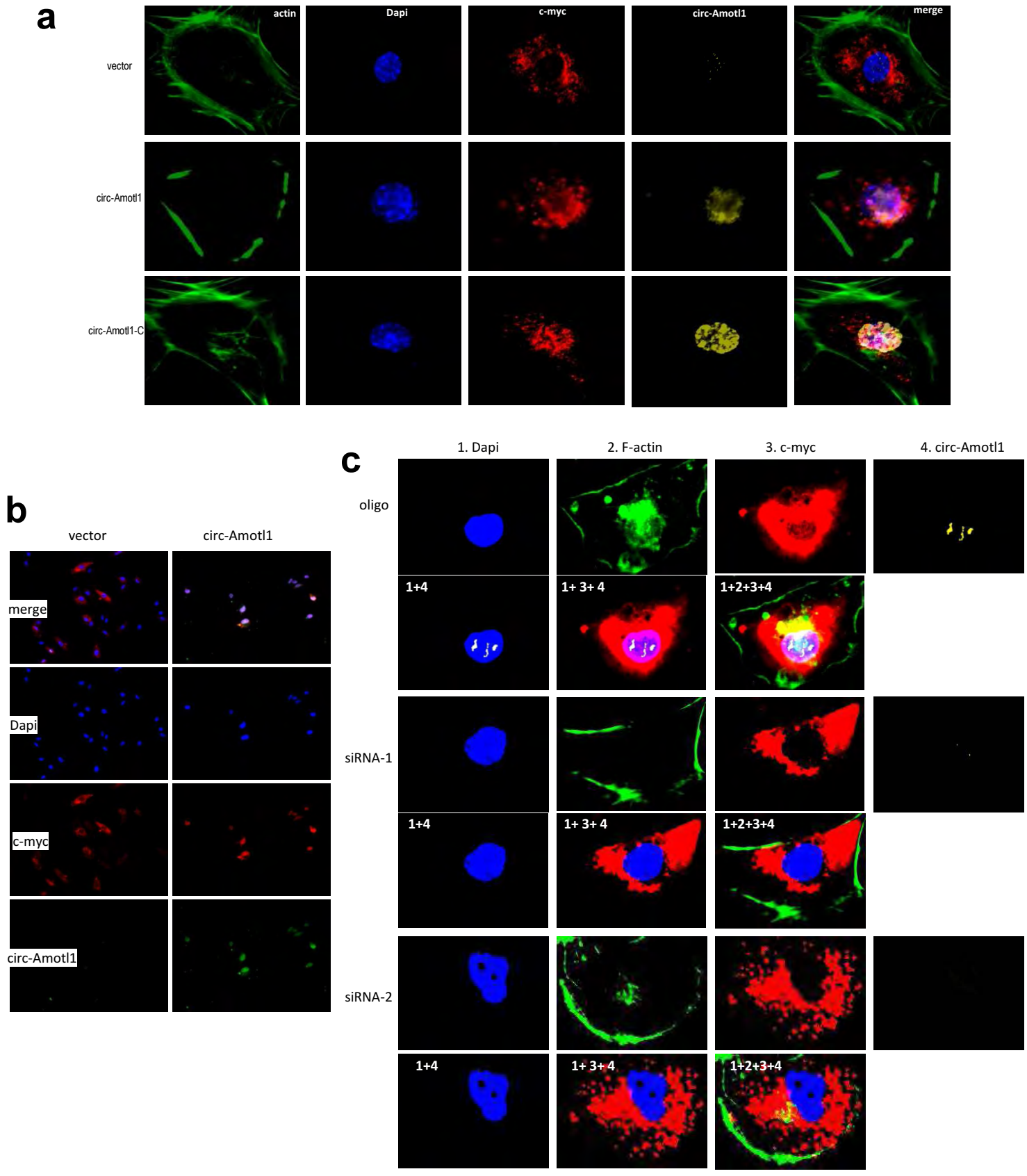

Fig S7. C-myc translocation affected by the siRNAs

(a) The cells were immuno-stained with phalloidins (green), DAPI (blue), c-myc (red), and circ-Amotl1 (yellow). Circ-Amotl1 was mainly detected in the nucleus of the circ-Amotl1-transfected cells.

(b) Field image of cells transfected with circ-Amotl1 or the vector showing co-localization of c-myc with circ-Amotl1 in the nuclei.

(c) The control oligo- and circ-Amotl1 siRNA-transfected MAD-MB-231 cells were stained with phalloidins (green), DAPI (blue), c-myc (red), and circ-Amotl1 (yellow). Silencing circ-Amotl1 depleted c-myc expression in the nucleus.

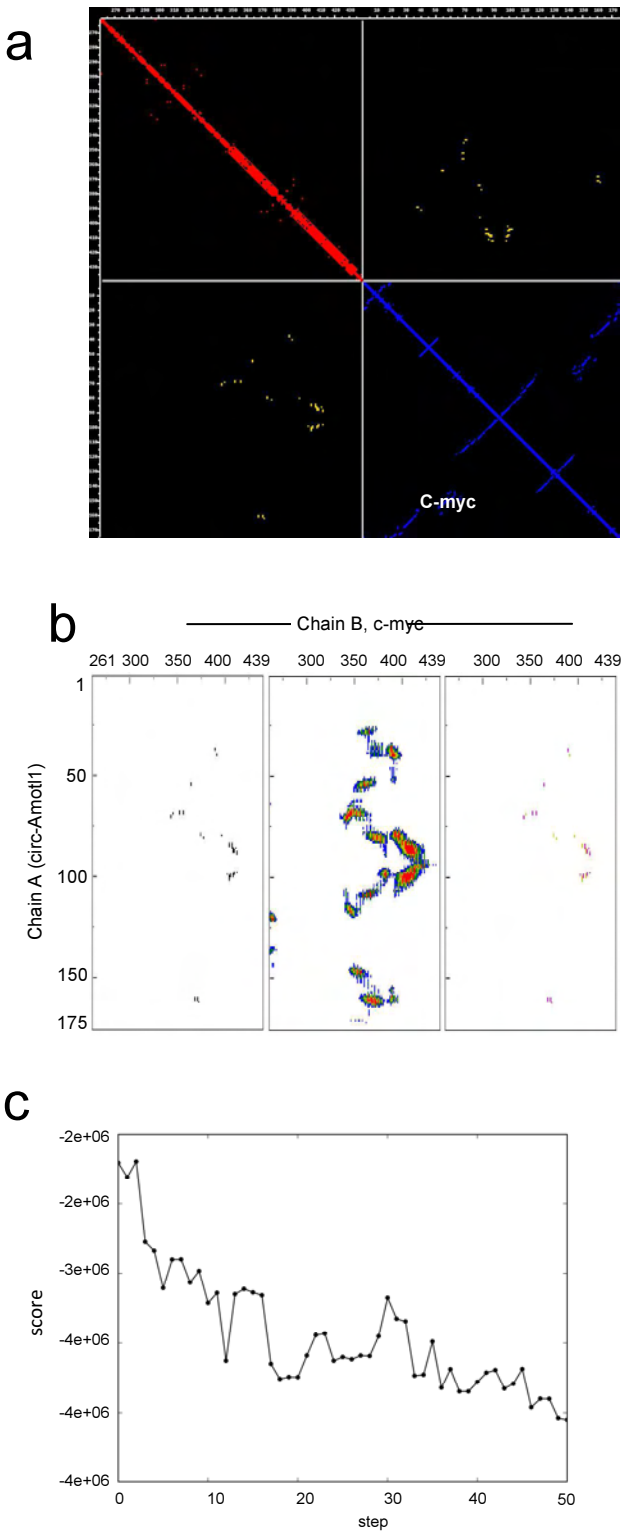

Fig S8. Computational analysis of circ-Amotl1 interacting with c-myc
(a) The contact map in the binding residues between circ-Amotl1 and c-myc.
(b) The residue-level resolution contact maps in the binding residues between circ-Amotl1 and c-myc.
(c) Refinement of the best docked circ-Amotl1-c-myc model showing MC score vs. steps of simulation.

Table S1. Circ-Amotl-1 expression with spike-in mouse RNA

Sample	Ct-human circAmotl1	Ct-mouse GAPDH	ΔCt	AVE	ΔΔCt	normalization	average	SD
vector-1	29.36	24.05	5.31		-0.26	1.20		
vector-2	29.17	23.33	5.84		0.27	0.83		
vector-3	29.14	23.53	5.61		0.04	0.97		
vector-4	28.95	23.43	5.52	5.57	-0.05	1.04	1.01	0.15
circAmotl-1	26.51	23.32	3.19		-2.38	5.21		
circAmotl-2	26.38	23.69	2.69		-2.88	7.36		
circAmotl-3	26.17	23.60	2.57		-3.00	8.00		
circAmotl-4	26.71	23.18	3.53	3.00	-2.04	4.11	6.17	1.82
vector+RNaseR-1	28.67	23.61	5.06		-0.51	1.42		
vector+RNaseR-2	29.47	23.71	5.76		0.19	0.88		
vector+RNaseR-3	29.61	23.82	5.79		0.22	0.86		
vector+RNaseR-4	28.54	23.15	5.39	5.50	-0.18	1.13	1.07	0.27
circAmotl1+RNaseR-1	26.20	23.28	2.92		-2.65	6.28		
circAmotl1+RNaseR-2	26.38	23.31	3.07		-2.50	5.66		
circAmotl1+RNaseR-3	26.01	23.31	2.70		-2.87	7.31		
circAmotl1+RNaseR-4	25.71	22.74	2.97	2.92	-2.60	6.06	6.33	0.70

Table S2. Circ-Amotl-1 expression without spike-in mouse RNA

Sample	Ct-human circAmotl1	Ct-human GAPDH	ΔCt	AVE	ΔΔCt	normalization	average	SD
vector-1	28.93	23.86	5.07		-0.50	1.41		
vector-2	29.15	23.50	5.65		0.08	0.95		
vector-3	29.18	23.42	5.76		0.19	0.88		
vector-4	29.41	24.05	5.36	5.46	-0.21	1.16	1.10	0.24
circAmotl-1	26.62	23.62	3.00		-2.57	5.94		
circAmotl-2	26.34	23.94	2.40		-3.17	9.00		
circAmotl-3	26.33	23.57	2.76		-2.81	7.01		
circAmotl-4	26.81	23.51	3.30	2.87	-2.27	4.82	6.69	1.78
vector+RNaseR-1	28.87	23.86	5.01		-0.56	1.47		
vector+RNaseR-2	28.95	23.50	5.45		-0.12	1.09		
vector+RNaseR-3	29.01	23.42	5.59		0.02	0.99		
vector+RNaseR-4	28.92	24.05	4.87	5.23	-0.70	1.62	1.29	0.31
circAmotl1+RNaseR-1	26.43	23.62	2.81		-2.76	6.77		
circAmotl1+RNaseR-2	26.81	23.94	2.87		-2.70	6.50		
circAmotl1+RNaseR-3	26.73	23.57	3.16		-2.41	5.31		
circAmotl1+RNaseR-4	26.02	23.51	2.51	2.84	-3.06	8.34	6.73	1.24

Table S3. The circ-Amotl1-c-myc Distance

N(res No)	atom	chain	AA (res No)	atom	chain	distance	type
U 37	O2'	A	LYS 389	CE	B	1.75	Phil phil
C 38	C5'	A	LYS 389	CE	B	2.94	Phil phil
U 40	OP1	A	PRO 391	CB	B	3.48	Phil phob
G 54	O3'	A	ARG 364	NH1	B	3.04	Phil phil
U 55	OP1	A	ARG 364	NH1	B	2.42	Phil phil
U 68	O3'	A	ARG 356	NH1	B	3.14	Phil phil
U 68	O3'	A	GLU 352	OE2	B	3.14	Phil phil
U 69	O2'	A	PRO 345	CA	B	2.66	Phil phob
U 69	OP1	A	GLU 352	OE2	B	2.63	Phil phil
U 69	OP1	A	ARG 356	NH1	B	1.65	Phil phil
C 70	C5'	A	THR 343	CG2	B	1.46	Phil phil
C 71	OP1	A	THR 343	OG1	B	2.46	Phil phil
C 79	O3'	A	PHE 374	CZ	B	3.31	Phil phob
G 80	C5'	A	PHE 374	CZ	B	1.98	Phil phob
G 80	OP2	A	LEU 396	CD2	B	2.85	Phil phob
G 81	OP1	A	LEU 377	CD1	B	2.01	Phil phob
G 84	N7	A	GLN 407	NE2	B	3.12	Phil phil
G 84	O6	A	LEU 404	CD2	B	2.63	Phil phob
C 85	N4	A	GLN 407	CB	B	2.05	Phil phil
C 85	N4	A	LEU 404	O	B	2.89	Phil phob
U 86	C5	A	GLN 411	NE2	B	0.87	Phil phil
U 86	O4	A	GLN 407	C	B	3.16	Phil phil
U 86	O4	A	ALA 408	CA	B	2.1	Phil phob
G 87	O6	A	ALA 408	CB	B	1.19	Phil phob
G 87	O6	A	GLU 409	N	B	3.16	Phil phil
G 88	O6	A	ALA 408	O	B	2.81	Phil phob
G 88	O6	A	LYS 412	CE	B	0.99	Phil phil
G 88	O6	A	GLU 409	N	B	3.34	Phil phil
A 89	N6	A	LYS 412	NZ	B	3.23	Phil phil
G 98	C6	A	GLU 409	OE2	B	1.17	Phil phil
G 98	O6	A	LYS 412	NZ	B	1.64	Phil phil
C 99	N4	A	ALA 408	C	B	2.96	Phil phob
C 99	OP2	A	TYR 402	CD1	B	3	Phil phil
C 99	N4	A	GLU 409	N	B	2.31	Phil phil
C99	N4	A	SER 405	O	B	1.88	Phil phil
A 100	N6	A	ALA 408	CB	B	1.99	Phil phob
A 100	N6	A	LEU 404	O	B	3.28	Phil phob
A 100	OP2	A	SER 405	OG	B	2.89	Phil phil
G 101	O6	A	LEU 404	CB	B	2.99	Phil phob
C 102	N4	A	LEU 404	CD2	B	1.39	Phil phob
A 160	O3'	A	LYS 371	NZ	B	1.95	Phil phil
A 160	O3'	A	ASN 368	OD1	B	2.22	Phil phil
G 161	C5'	A	LYS 371	CE	B	0.71	Phil phil
G 161	OP1	A	ASN 368	OD1	B	0.7	Phil phil
U 162	OP1	A	ARG 372	CG	B	3.44	Phil phil

The table reporting a list of atoms “in contact” (within the distance cutoff) with relative distances less than 3.5Å.

Table S4. Accessible Surface Area table of circ-Amolt1-c-myc complex

Buried area upon the complex formation (A^2) 3321.0
Buried area upon the complex formation (%) 6.92
Interface area (A^2) 1660.5
Interface area circ-AMOTL1 (%) 5.56
Interface area c-Myc (%) 9.16
POLAR Buried area upon the complex formation (A^2) 1611.2
POLAR Interface (%) 48.52
POLAR Interface area (A^2) 805.6
NON POLAR Buried area upon the complex formation (A^2) 1709.9
NON POLAR Interface (%) 51.49
NON POLAR Interface area (A^2) 854.95
Residues at the interface_total (n) 90
Residues at the interface_circ-AMOTL1 43
Residues at the interface_c-Myc 47

Table S5. circ-Amolt1-c-myc interaction overview

Number of interacting residues circ-AMOTL1 **26**
Number of interacting residues c-Myc **21**
Number of hydrophilic-hydrophobic interaction **16**
Number of hydrophilic-hydrophilic interaction **29**
Number of hydrophobic-hydrophobic interaction **0**